

The near vacuum hohlraum campaign at the NIF: A new approach

S. Le Pape, L. F. Berzak Hopkins, L. Divol, N. Meezan, D. Turnbull, A. J. Mackinnon, D. Ho, J. S. Ross, S. Khan, A. Pak, E. Dewald, L. R. Benedetti, S. Nagel, J. Biener, D. A. Callahan, C. Yeaman, P. Michel, M. Schneider, B. Koziowski, T. Ma, A. G. Macphee, S. Haan, N. Izumi, R. Hatarik, P. Sterne, P. Celliers, J. Ralph, R. Rygg, D. Strozzi, J. Kilkenny, M. Rosenberg, H. Rinderknecht, H. Sio, M. Gatu-Johnson, J. Frenje, R. Petrasso, A. Zylstra, R. Town, O. Hurricane, A. Nikroo, and M. J. Edwards

Citation: *Physics of Plasmas* **23**, 056311 (2016); doi: 10.1063/1.4950843

View online: <http://dx.doi.org/10.1063/1.4950843>

View Table of Contents: <http://scitation.aip.org/content/aip/journal/pop/23/5?ver=pdfcov>

Published by the *AIP Publishing*

Articles you may be interested in

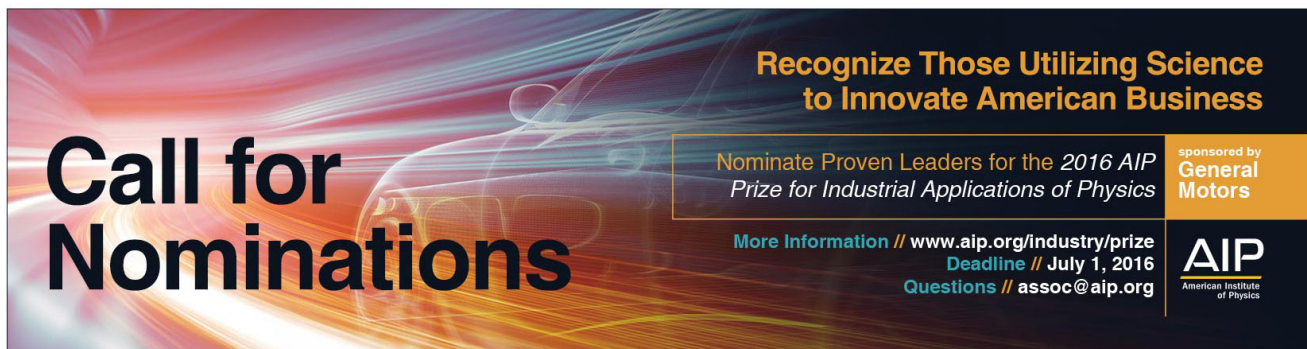
[The size and structure of the laser entrance hole in gas-filled hohlraums at the National Ignition Facility](#)
Phys. Plasmas **22**, 122705 (2015); 10.1063/1.4937369

[Point design targets, specifications, and requirements for the 2010 ignition campaign on the National Ignition Facility](#)
Phys. Plasmas **18**, 051001 (2011); 10.1063/1.3592169

[The effect of condensates and inner coatings on the performance of vacuum hohlraum targets](#)
Phys. Plasmas **17**, 032701 (2010); 10.1063/1.3334998

[Developing depleted uranium and gold cocktail hohlraums for the National Ignition Facility](#)
Phys. Plasmas **14**, 056310 (2007); 10.1063/1.2718527

[Calculation of re-emission diagnostic in NIF ignition Hohlraum at 1 MJ laser energy](#)
Rev. Sci. Instrum. **77**, 10E302 (2006); 10.1063/1.2217008



Call for Nominations

Recognize Those Utilizing Science to Innovate American Business

Nominate Proven Leaders for the 2016 AIP Prize for Industrial Applications of Physics

More Information // www.aip.org/industry/prize
Deadline // July 1, 2016
Questions // assoc@aip.org

sponsored by General Motors

AIP
American Institute of Physics

The near vacuum hohlraum campaign at the NIF: A new approach

S. Le Pape,^{1,a)} L. F. Berzak Hopkins,¹ L. Divol,¹ N. Meezan,¹ D. Turnbull,¹ A. J. Mackinnon,² D. Ho,¹ J. S. Ross,¹ S. Khan,¹ A. Pak,¹ E. Dewald,¹ L. R. Benedetti,¹ S. Nagel,¹ J. Biener,¹ D. A. Callahan,¹ C. Yeaman,¹ P. Michel,¹ M. Schneider,¹ B. Koziolowski,¹ T. Ma,¹ A. G. Macphee,¹ S. Haan,¹ N. Izumi,¹ R. Hatarik,¹ P. Sterne,¹ P. Celliers,¹ J. Ralph,¹ R. Rygg,¹ D. Strozzi,¹ J. Kilkenny,³ M. Rosenberg,¹ H. Rinderknecht,¹ H. Sio,⁴ M. Gatu-Johnson,⁴ J. Frenje,⁴ R. Petrasso,⁴ A. Zylstra,⁵ R. Town,¹ O. Hurricane,¹ A. Nikroo,¹ and M. J. Edwards¹

¹Lawrence Livermore National Laboratory, Livermore, California 94550, USA

²SLAC National Accelerator Laboratory, 2575 Sand Hill Road, MS 19, Menlo Park, California 94025, USA

³General Atomics, San Diego, California 92186, USA

⁴Plasma Science and Fusion Center, Massachusetts Institute of Technology, Cambridge, Massachusetts 02139, USA

⁵Los Alamos National Laboratory, Los Alamos, New Mexico 87545, USA

(Received 19 January 2016; accepted 23 February 2016; published online 25 May 2016)

The near vacuum campaign on the National Ignition Facility has concentrated its efforts over the last year on finding the optimum target geometry to drive a symmetric implosion at high convergence ratio ($30\times$). As the hohlraum walls are not tamped with gas, the hohlraum is filling with gold plasma and the challenge resides in depositing enough energy in the hohlraum before it fills up. Hohlraum filling is believed to cause symmetry swings late in the pulse that are detrimental to the symmetry of the hot spot at high convergence. This paper describes a series of experiments carried out to examine the effect of increasing the distance between the hohlraum wall and the capsule (case to capsule ratio) on the symmetry of the hot spot. These experiments have shown that smaller Case to Capsule Ratio (CCR of 2.87 and 3.1) resulted in oblate implosions that could not be tuned round. Larger CCR (3.4) led to a prolate implosion at convergence $30\times$ implying that inner beam propagation at large CCR is not impeded by the expanding hohlraum plasma. A Case to Capsule ratio of 3.4 is a promising geometry to design a round implosion but in a smaller hohlraum where the hohlraum losses are lower, enabling a wider cone fraction range to adjust symmetry. *Published by AIP Publishing.* [<http://dx.doi.org/10.1063/1.4950843>]

INTRODUCTION

Until recently, the approach to Inertial Confinement Fusion (ICF)¹ on the National Ignition Facility (NIF)² consisted of a 2 mm diameter CH capsule placed at the center of a gold hohlraum filled with helium at a density varying from 0.9 to 1.6 mg/cc with laser pulses ranging from 15 ns for the high foot design^{3,4} up to 21 ns for the low foot design.⁵ The purpose of the helium was to prevent the hohlraum from filling with ablated gold that would then block the propagation of laser beams into the hohlraum. With the development of High-Density Carbon (HDC)^{6–9} capsules, because of its higher density (3.4 versus 1.04 g/cc for CH), shorter laser pulses, of order 10 ns, become ignition relevant making the use of near vacuum hohlraums a viable option. Early during the National Ignition Campaign,¹⁰ vacuum hohlraums¹¹ were proven to be a high efficiency platform, but these initial experiments were carried out using 2 ns pulses, not ignition relevant. Over the last two years, we have realized experiments in near-vacuum hohlraums (NVH) with pulses ranging from 0.9 to 1.6 MJ and up to 9 ns long. The coupling from laser energy to hohlraum was measured consistently to be over 97%, with a minimal amount (10 J) of hot electrons

above 170 keV due to Laser Plasma Interaction (LPI). In addition, NVH have shown that the time varying coefficient¹² used to match the experimental data such as the burn average ion temperature and the bang time is on the order of 0.8–0.9 when applied at the peak of the laser pulse. In conclusion, NVH are a promising platform for ignition relevant pulses: LPI is minimal, the hot electron production above 170 keV is about 100 times lower than measured for comparable laser pulses in the gas filled hohlraums, the laser to hohlraum coupling stays over 97%. As the time varying coefficient used to match the experimental data is higher (0.72–0.78 typically for gas filled hohlraum versus 0.8–0.9 for NVH), NVH are overall 30% more efficient than gas filled hohlraum.¹³ Symmetry of implosions driven with the NVH is controlled through direct adjustments to the inner and outer beam power balance (cone fraction) rather than relying on beam wavelength separations¹⁴ and the resultant cross-beam energy transfer.^{15,16} Because cross-beam transfer is dictated by plasma conditions,¹⁵ the amount of cross-beam transfer is density- and temperature-dependent and, hence, time-dependent and not directly controlled. Nevertheless, the challenge in NVH is also symmetry control of the hot spot. As the hohlraum walls are not tamped by the helium gas, laser beam propagation is impeded at late time by the expanding plasma. Figure 1 shows a map of the laser intensity at two different times (5 and 6 ns from the beginning of

Note: Paper GI3 1, Bull. Am. Phys. Soc. **60**, 111 (2015).

^{a)}Invited speaker.

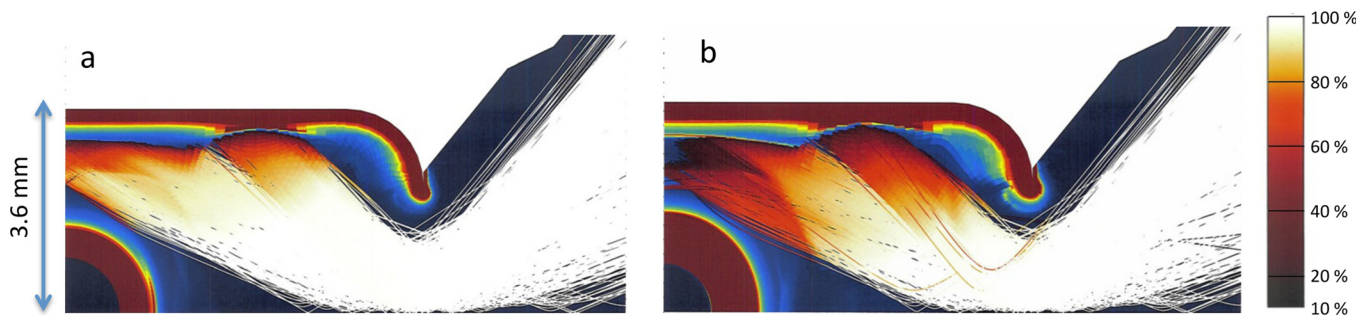


FIG. 1. Map of laser beam intensity in a NVH hohlraum. (a) Laser intensity 5 ns after the beginning of the laser pulse; (b) laser intensity 6 ns after the beginning of the laser pulse.

the laser pulse). At 5 ns, the laser is still reaching the hohlraum wall, while at 6 ns, it starts to be absorbed in the expanding gold. The consequence of this is the loss of symmetry control, as the capsule is only partially imploded, characterized by a positive symmetry swing starting at 6 ns (Figure 2, P2/P0 curve, black curve).

To mitigate this effect, the strategy pursued was to vary the distance from the hohlraum wall to the capsule giving more time to the beam to reach the wall. The limit in making the hohlraum larger is the laser energy available. As the hohlraum gets larger from 5.75 to 6.2 to 6.72 mm diameter, the wall surface increases, meaning that the laser power needed to reach the same peak radiative temperature also increases; for example, to reach a 300 eV peak T_r , 380 TW are needed in a 5.75 hohlraum, 420 TW in a 6.20 hohlraum, and 480 TW in a 6.72 hohlraum. In this paper, we will first present results on a series of experiments carried out in a 5.75 and 6.2 hohlraum that resulted in oblate implosions that could not be tuned round with this capsule and hohlraum combination. Symmetry in the larger hohlraum (6.72) was then explored, and a series of experiments aimed at tuned shell and hot spot symmetry using cone fraction will be presented. This series resulted in a prolate implosion, suggesting that the optimum geometry to achieve a round hot spot is

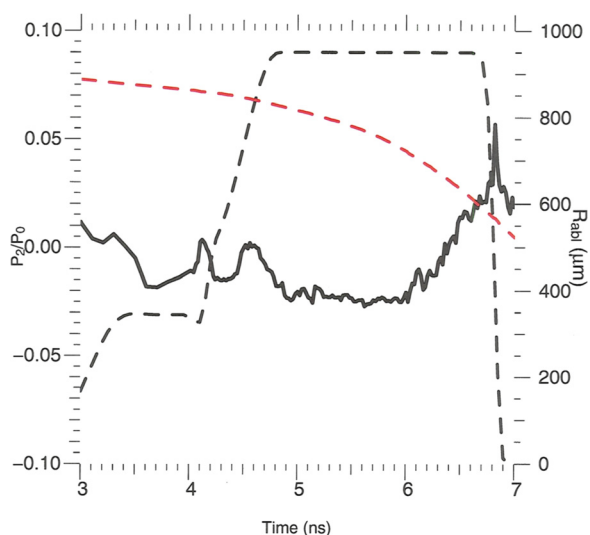


FIG. 2. Red dashed curve: shell position as a function of time; black dashed curve: laser pulse (peak laser power is 350 TW); black curve: P2/P0 as a function of time.

between a 6.72 and a 6.2 hohlraum with a 2 mm diameter capsule.

EXPERIMENTAL TECHNIQUES AND MEASURES

The National Ignition Facility (NIF) is a 192 beams laser system with a maximum energy of 1.8 MJ. The 192 beams are split between 64 inner beams and 128 outer beams; inner beams are aimed at the waist of the hohlraum, and outer beams are aimed above and under the hohlraum waist. The inherent inner cone fraction (defined as the inner cone power divided by the total power) of the NIF is thus one third. The experiments described here use a 28 μm thick gold hohlraum with a 2 mm inner diameter undoped HDC capsule placed at its center; during the course of these experiments, the thickness of the HDC capsule was varied from 85 to 78 μm while keeping its inner diameter identical. To vary the Case to Capsule Ratio (CCR), the size of the hohlraum was changed from a standard 5.75 mm diameter, 10.1 mm long hohlraum to a 6.2 mm, 10.92 mm length hohlraum, and finally, a 6.72 mm, 11.24 mm length hohlraum (Figure 3). The hohlraum was filled with 0.032 mg/cc of helium, the minimum amount of helium required to provide conduction cooling of the capsule to enable the growth of DT layers.

In this paper, we will describe three different types of experiments: (a) SYMCAPS,¹⁶ (b) 2DCONA,¹⁷ and (c) DT layered implosion.¹⁸ For SYMCAPS experiments described in this paper, the HDC capsule was filled with 8 mg/cc of DHe3 at 32 K, the convergence ratio (CR) (i.e., ratio of the initial inner diameter to the hot spot P0) is about 15 \times . 2DCONA experiments provide a 2D backlit image of the imploding shell as a function of time at a convergence ratio of about 4, and the shell backlighter is an iron foil at 6.4 keV. The 2DCONA targets have hohlraum windows on either side of the capsule, and a backlighter foil is chosen to give the optimum contrast to measure the shape and density of the ablator. On DT layered implosions, a 58 μm thick DT layer is formed on the inner surface of the HDC capsule.^{19,20} The convergence ratio is of order 30 \times . This paper focuses on shape control of the shell and hot spot as a function of target geometry and laser cone fraction. The principal X-ray imaging diagnostics are Gated X-ray Detectors (GXD),²¹ which take multiple time-resolved images of either (a) the self-emission of the imploding capsule (Symcap, DT layered implosion) or (b) a 2D backlit image of the imploding shell (2DCONA). The X-ray framing cameras used to record

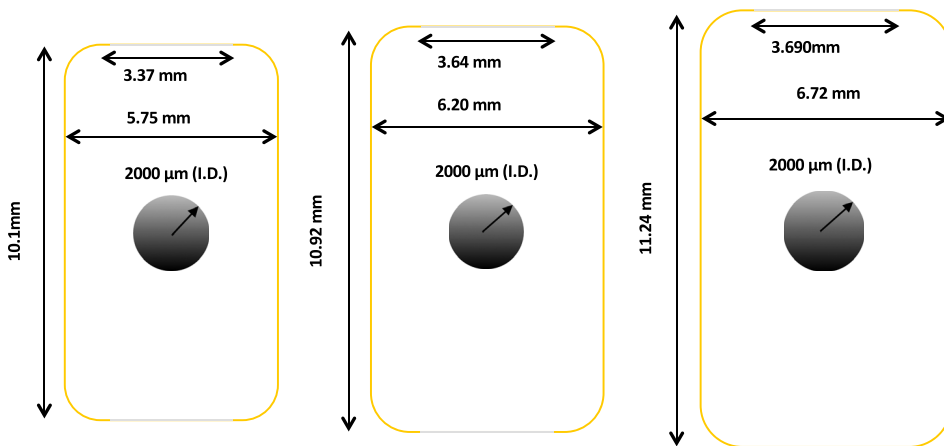


FIG. 3. Target geometries for the experiments described in this paper. (a) 5.75 hohlraum with a 2 mm capsule, CCR = 2.81; (b) 6.20 hohlraum with a 2 mm capsule, CCR = 3.4; (c) 6.72 mm hohlraum with a 2 mm capsule, CCR = 3.4.

self-emission or backlit images have a spatial resolution of $\sim 10 \mu\text{m}$ and a temporal resolution of 80 ps; on SYMCAPS, the kapton filter cuts X-rays below 5 keV. The shapes of the imploding shell and self-emission obtained from the GXD are both sensitive indicators of the symmetry of the X-ray drive.

SYMMETRY CONTROL IN 5.75 mm AND 6.20 mm HOHLRAUMS

The laser pulse used to drive the 85 μm capsule is a 3 shock pulse,²² 8.7 ns long 1.3 MJ, resulting in an implosion adiabat of ~ 2.2 (Figure 4). We first tested this pulse shape in a 5.75 hohlraum at a CCR of 2.875.

Figure 4 shows the equatorial X-ray image on the hot spot at bang time (SYMCAP shot number N141019). The measured hot spot is strongly oblate with a central emitting spot of $\sim 45 \mu\text{m}$ P0. The presence and size of a central

small hot spot are consistent with polar jets. 2D HYDRA²³ post-shot simulations using empirical model adjustment²⁴ are consistent with this scenario. Figure 5 shows both a simulation of the equatorial X-ray image of the hot spot at bang time and the corresponding 2D map of the density. The simulated X-ray image shows the same characteristic as the experimental one, an oblate implosion with a small bright emission spot at its center. From the 2D map of the density at bang time (Figure 5(b)), the bright small spot is induced by the density buildup on the poles collapsing on the hot spot at bang time. The conclusion from this experiment was that the laser pulse was too long to drive a 3 shock pulse shape in a 5.75 hohlraum (CCR = 2.875), late time P2/P0 positive swing caused by hohlraum fillings being responsible for the polar jets. The same pulse was then tested in a larger hohlraum, 6.2 hohlraum (CCR = 3.1), to give more time to the laser to deposit its energy in the hohlraum before it closes.

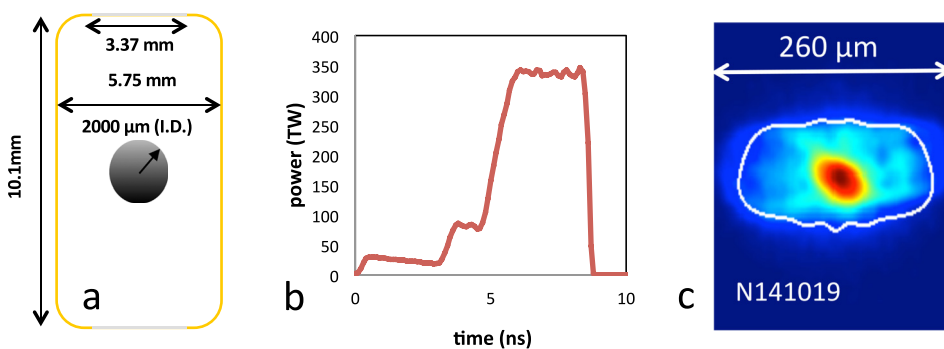


FIG. 4. (a) Target geometry, (b) 3 shock laser pulse, (c) equatorial X-ray image of the hot spot at bang time for N141019 shot. White contour is the 17% of the peak brightness contour.

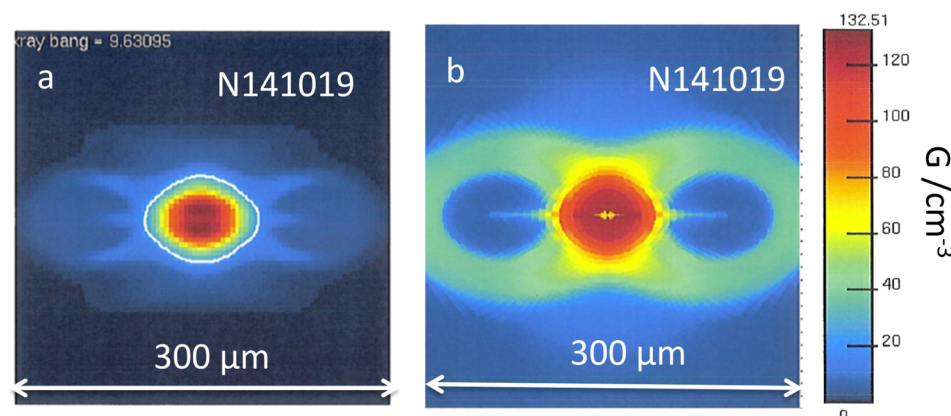


FIG. 5. (a) HYDRA simulation of N141019 equatorial X-ray image at bang time. (b) Corresponding 2D HYDRA simulation of the density at bang time. White contour is the 17% of the peak brightness contour.

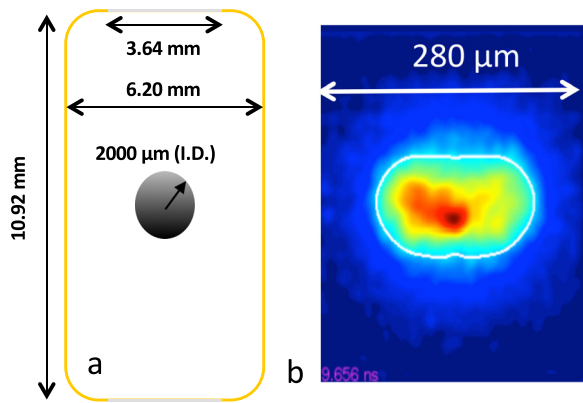


FIG. 6. (a) Target geometry. (b) Equatorial X-ray image of the hot spot at bang time for N150128 shot. White contour is the 17% of the peak brightness contour.

Figure 6 shows the equatorial image of the hot spot emission at bang time. The measured hot spot is still oblate, but the measured P_0 ($71.5 \mu\text{m}$) is now in line with the expected convergence of a SYMCAp ($\sim 15\times$), while the symcap is still oblate ($P_2/P_0 = -42\%$). Post-shot simulations (Figure 7) capture the symmetry improvement going to a larger CCR, and the simulated equatorial hot spot emission

is consistent with the observed hot spot, but the 2D density map (Figure 7(b)) shows that significant density buildups are still present on the poles that would induce a pinch of the hot spot going to a higher convergence DT layered shot.

SYMMETRY CONTROL IN A 6.72 mm HOHLRAUM

A mini-tuning campaign was carried out in the 6.72 hohlraum leading to DT layered shot. Two keyhole shots (N140130, N140429) were performed to adjust the shock timing, two 2DconA (N140213, N140702) to look at the symmetry of the shell and hot spot at low convergence (up to $\sim 15\times$) and two DT layered shots (N140929, N151007) to assess the performance of high convergence shots.²⁴ As the symmetry of the implosion was consistently prolate on 2DconA shots (N140213 and N140702, Figure 8), the laser pulse length (Figure 9) was gradually increased from 6.8 to 7.6 to 8.1 (on N140926), as the HYDRA pre-shot simulations predicted that going to a longer pulse would result in a more oblate hot spot due to late time filling of the hohlraum. Increasing the pulse length from 6.8 to 7.6 ns did not change the symmetry of the hot spot, suggesting that the inner beams are still freely propagating to the waist of the hohlraum.

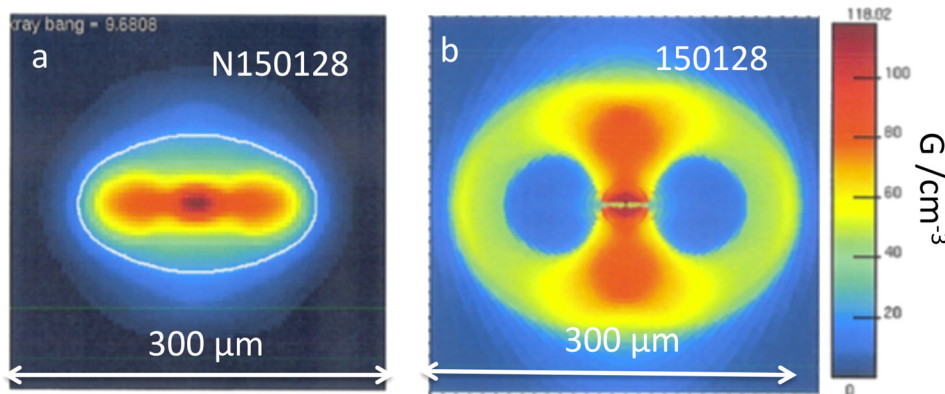


FIG. 7. (a) HYDRA simulation of N150128 equatorial X-ray image at bang time. (b) Corresponding 2D HYDRA simulation of the density at bang time. White contour is the 17% of the peak brightness contour.

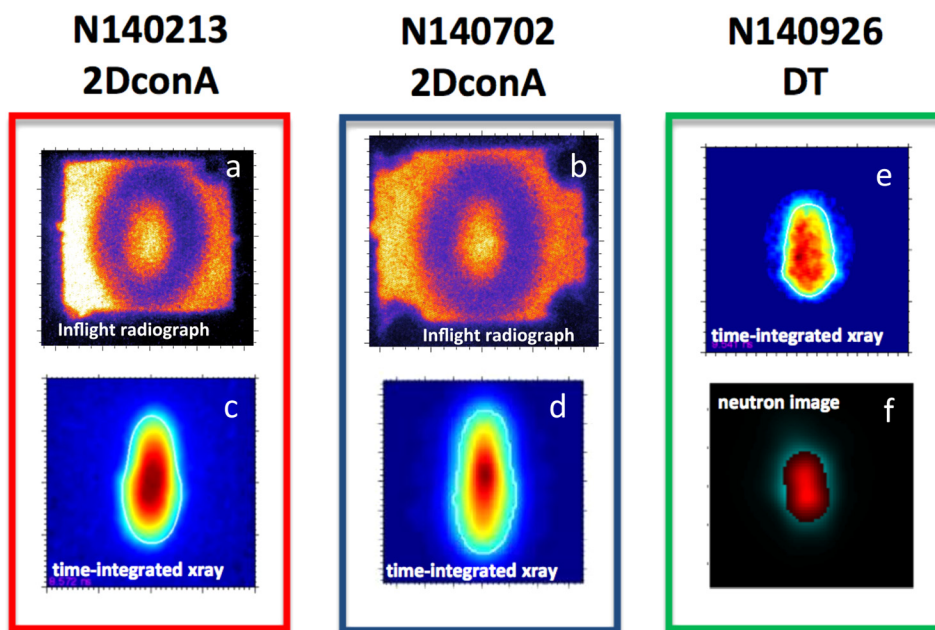


FIG. 8. Comparison of radiographs (a, b), equatorial X-ray images (c, d, e), and equatorial neutron images (f). The radiographs are shown in $800 \times 800 \mu\text{m}$ scale; equatorial images are shown in $150 \times 150 \mu\text{m}$ scale. Equatorial neutron image is shown in $100 \times 100 \mu\text{m}$ scale.

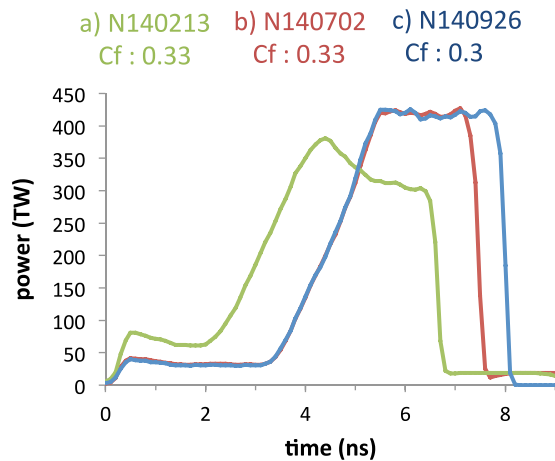


FIG. 9. Laser pulse shape: (a) 2DconA N140213, (b) 2DconA N140702, (c) DT cryogenic implosion N140926.

On N140926, in addition to lengthening the pulse, the cone fraction was changed from 33% to 30% (Figure 9); this change in cone fraction is intended to reduce laser energy deposition at the waist of the hohlraum to drive a less prolate implosion. The hot spot P2 went from 35 μm prolate on N140702 to 10 μm prolate on N140926 (Figure 10). On the following DT layered shot, N151007, to adjust the hot spot shape, the cone fraction was changed from 30% to 25% by reducing the inner beam power as opposed to increasing the outer beam power, because the outer beams were already at their 1.8 MJ full NIF equivalent energy. This significant change in cone fraction did not result in a change in symmetry of the hot spot (Table I); change in neutron yield is attributed to a somewhat slower implosion velocity caused by a lower total laser energy on N151007.

These results were unexpected considering the change of hot spot symmetry previously observed going from the 2DconA (N140702) to the DT layered shot (N140926)

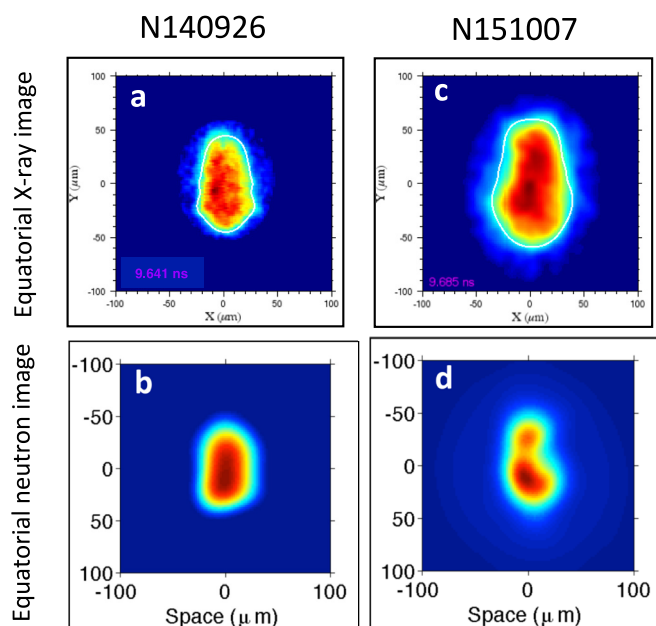


FIG. 10. Comparison of equatorial X-ray images (a), (c) and equatorial neutron images (b), (d) for N140926 (a), (b) and N151007 (c), (d).

TABLE I. Implosion performance and laser pulse for 6.72 mm DT layered implosions.

	N140926	N151007
Laser energy (MJ)	1.6	1.54
Laser power (TW)	425	397
Bang time (ns)	9.65	9.67
Neutron yield	2.85×10^{15}	1.54×10^{15}
Coast time (ns)	~ 2	~ 2
DT Tion (keV)	3.9	3.83
DD Tion (keV)	3.9	3.6
DSR (%)	2.74	2.17
Peak laser C. F.	0.3	0.25
P0 (μ)	30.6	41.9
P2 (μ)	12.5	13.1

(Figure 10). We observed a 25 μm P2 changed between these 2 shots, while P2 did not change between the 2 DT layered shots. The change in P2 between the first two shots could be attributed to three factors: (1) a longer pulse length that tended to drive an oblate implosion, (2) a change in cone fraction (from 33% to 30%), (3) a different shell trajectory due to the presence of the 58 μm DT layer. The mass of the shell + DT layer (41.2 mg) is higher than the mass of the shell itself (39.5 mg), causing the shell to spend more time at higher radius before converging. Between the two DT shots, only the cone fraction at the peak of the pulse was changed (from 30% to 25%), but the hot spot symmetry did not change. In addition to the prolate asymmetry (P2), a vertical (top/down) asymmetry was observed (in this case, this asymmetry could be induced by a vertical shift of the initial position of the capsule of about 40 μm) which could affect the P2 observed.

CONCLUSION

A series of experiments have been carried out on the NIF to investigate symmetry control in Near Vacuum Hohlraums. The Near Vacuum Hohlraum platform has proven over a wide laser energy range to be a low LPI, high efficiency platform capable of driving ignition relevant pulses with HDC capsules. The challenge in NVH is symmetry control as the hohlraum fills late in time with abated material. As the hohlraum fills with gold, inner beam propagation is impeded causing a late time symmetry swing of the X-ray flux on the capsule. To mitigate this issue, we have explored three different Case to Capsule Ratios on the basis that a larger distance between the capsule and the wall assists late time inner beam propagation. Three shock ignition relevant pulse shapes in $15\times$ convergence experiments have led to oblate, pinching implosions at CCR of 2.85 and 3.1. Late time X-ray symmetry swing causes density buildup at the poles, pinching the hot spot at peak convergence.

A tuning campaign has been carried out in a larger CCR = 3.4 (6.72 mm hohlraum with a 2 mm ID HDC capsule) target geometry leading to 2 cryogenic implosions. 2DconA experiments have shown that the shell was prolate early during the implosion; high convergence DT implosions have shown that both the neutron image and the X-ray

images of the hot spot are also prolate. The cryogenic implosions (N140926, N151007) resulted in neutron yields of $\sim 1.5\text{--}3 \times 10^{15}$ at a burn average temperature of 3.9 keV. Due to the energy limitations of the laser (≤ 1.8 MJ, full NIF equivalent), we were not able to tune the hot spot to round in this 6.72 hohlraum.

Ongoing work is focused toward the 3.4 CCR geometry but in a smaller hohlraum. Because of the large wall surface area in the 6.72 hohlraum, the laser power needed to reach $\sim 280\text{--}300$ eV radiation temperature is too limiting for the cone fraction range we can use to tune the hot spot symmetry. A 5.75 hohlraum with a smaller capsule (0.8 versus 1 mm inner radius) has the same CCR but the power needed to reach similar peak radiative temperatures is lower, providing the cone fraction range needed to tune symmetry. Other options that we have not explored yet but are in future plans are the use of unlined Uranium hohlraums²⁵ which are proven to be $\sim 6.5\%$ more efficient than gold hohlraums and adding a small amount of helium gas (0.1–0.3 mg/cc) to control the hohlraum wall expansion while staying under the density onset for LPI.

ACKNOWLEDGMENTS

This work was performed under the auspices of the U.S. Department of Energy by Lawrence Livermore National Laboratory under Contract No. DE-AC52-07NA27344. Work was also supported by the Laboratory Directed Research and Development Grant No. 11-ERD-050 and the National Laboratory User Facility.

¹J. D. Lindl, P. Amendt, R. L. Berger, S. G. Glendinning, S. H. Glenzer, S. W. Haan, R. L. Kauffman, O. L. Landen, and L. J. Suter, *Phys. Plasmas* **11**, 339 (2004).

²E. Moses, R. Boyd, B. Remington, C. Keane, and R. Al-Ayat, *Phys. Plasmas* **16**, 041006 (2009).

³T. Dittrich, O. Hurricane, D. Callahan, E. Dewald, T. Döppner, D. Hinkel, L. B. Hopkins, S. Le Pape, T. Ma, J. Milovich *et al.*, *Phys. Rev. Lett.* **112**, 055002 (2014).

⁴O. Hurricane, D. Callahan, D. Casey, P. Celliers, C. Cerjan, E. Dewald, T. Dittrich, T. Döppner, D. Hinkel, L. B. Hopkins *et al.*, *Nature* **506**, 343 (2014).

⁵M. Edwards, P. Patel, J. Lindl, L. Atherton, S. Glenzer, S. Haan, J. Kilkenny, O. Landen, E. Moses, A. Nikroo *et al.*, *Phys. Plasmas* **20**, 070501 (2013).

⁶J. Biener, D. D. Ho, C. Wild, E. Woerner, and M. M. Biener, *Nuclear Fusion* **49**(11), 112001 (2009).

⁷J. S. Ross *et al.*, *Phys. Rev. E* **91**, 021101 (2015).

⁸A. J. Mackinnon, N. B. Meezan, J. S. Ross, S. Le Pape, L. B. Hopkins, L. Divol, D. Ho, J. Milovich, A. Pak, J. Ralph *et al.*, *Phys. Plasmas* **21**, 056318 (2014).

⁹N. B. Meezan, L. F. B. Hopkins, S. Le Pape, L. Divol, A. J. Mackinnon, T. Doppner, D. D. Ho, O. S. Jones, S. F. Khan, T. Ma *et al.*, *Phys. Plasmas* **22**, 062703 (2015).

¹⁰J. Lindl, O. Landen, J. Edwards, E. Moses, N. Team *et al.*, *Phys. Plasmas* **21**, 020501 (2014).

¹¹R. E. Olson, L. J. Suter, J. L. Kline, D. A. Callahan, M. D. Rosen, S. N. Dixit, O. L. Landen, N. B. Meezan, J. D. Moody, C. A. Thomas *et al.*, *Phys. Plasmas* **19**, 053301 (2012).

¹²O. S. Jones, C. J. Cerjan, M. M. Marinak, J. L. Milovich, H. F. Robey, P. T. Springer, L. R. Benedetti, D. L. Bleuel, E. J. Bond, D. K. Bradley *et al.*, *Phys. Plasmas* **19**, 056315 (2012).

¹³L. B. Hopkins, N. Meezan, S. Le Pape, L. Divol, A. Mackinnon, D. Ho, M. Hohenberger, O. Jones, G. Kyrala, J. Milovich *et al.*, *Phys. Rev. Lett.* **114**, 175001 (2015).

¹⁴P. Michel, L. Divol, E. Williams, S. Weber, C. Thomas, D. Callahan, S. Haan, J. Salmonson, S. Dixit, D. Hinkel *et al.*, *Phys. Rev. Lett.* **102**, 025004 (2009).

¹⁵P. Michel, S. Glenzer, L. Divol, D. Bradley, D. Callahan, S. Dixit, S. Glenn, D. Hinkel, R. Kirkwood, J. Kline *et al.*, *Phys. Plasmas* **17**, 056305 (2010).

¹⁶G. Kyrala, J. Kline, S. Dixit, S. Glenzer, D. Kalantar, D. Bradley, N. Izumi, N. Meezan, O. Landen, D. Callahan *et al.*, *Phys. Plasmas* **18**, 056307 (2011).

¹⁷J. Rygg, O. Jones, J. Field, M. Barrios, L. Benedetti, G. Collins, D. Eder, M. Edwards, J. Kline, J. Kroll *et al.*, *Phys. Rev. Lett.* **112**, 195001 (2014).

¹⁸S. Glenzer, D. Callahan, A. MacKinnon, J. Kline, G. Grim, E. Alger, R. Berger, L. Bernstein, R. Betti, D. Bleuel *et al.*, *Phys. Plasmas* **19**, 056318 (2012).

¹⁹J. Sater, B. Koziowski, G. W. Collins, E. Mapoles, J. Pipes, J. Burmann, and T. Bernat, *Fusion Technol.* **35**, 229 (1999).

²⁰B. Koziowski, J. Koch, A. Barty, H. Martz, Jr., W.-K. Lee, and K. Fezzaa, *J. Appl. Phys.* **97**, 063103 (2005).

²¹G. Kyrala, S. Dixit, S. Glenzer, D. Kalantar, D. Bradley, N. Izumi, N. Meezan, O. Landen, D. Callahan, S. Weber *et al.*, *Rev. Sci. Instrum.* **81**, 10E316 (2010).

²²D. Ho, S. Haan, J. Salmonson, L. Benedict, J. Biener, and M. Herrmann, in *APS Meeting Abstracts* (2009), p. 5015.

²³M. M. Marinak, G. D. Kerbel, N. A. Gentile, O. Jones, D. Munro, S. Pollaine, T. R. Dittrich, and S. W. Haan, *Phys. Plasmas* **8**, 2275 (2001).

²⁴L. B. Hopkins, S. Le Pape, L. Divol, N. Meezan, A. Mackinnon, D. Ho, O. Jones, S. Khan, J. Milovich, J. Ross *et al.*, *Phys. Plasmas* **22**, 056318 (2015).

²⁵J. Kline, D. Callahan, S. Glenzer, N. Meezan, J. Moody, D. Hinkel, O. Jones, A. MacKinnon, R. Benedetti, R. Berger *et al.*, *Phys. Plasmas* **20**, 056314 (2013).